Early reactivity of sodium silicate-activated slag pastes and its impact on rheological properties

M. Palacios, S. Gismera, M.M. M Alonso, Jean-Baptiste D'espinose de Lacaillerie, B. Lothenbach, A. Favier, C. Brumaud, F. Puertas

Early reactivity of sodium silicate-activated slag pastes and its impact on rheological properties

M. Palacios [a,*], S. Gismera [a], M.M. Alonso [a], J.B. d'Espinose de Lacaillerie [b], B. Lothenbach [c], A. Favier [d], C. Brumaud [d], F. Puertas [a]

[a] Eduardo Torroja Institute for Construction Science (IETcc-CSIC), Madrid, Spain
[b] Soft Matter Science and Engineering Laboratory (SIMM), UMR CNRS 7615, Université PSL, ESPCI Paris, Paris, France
[c] Concrete and Construction Chemistry, EMPA, Zurich, Switzerland
[d] Chair of Sustainable Construction, ETHZ, Zurich, Switzerland

ARTICLE INFO

Keywords:
Alkali-activated slag cement
Sodium silicate activator
Rheology
Reaction
Thermodynamic calculations

ABSTRACT

The fast loss of fluidity of sodium silicate-activated slag (SS-AAS) systems have been widely studied in the literature. In this study, the rheology of these cements has been correlated with the evolution of the reaction products formed over time. For this purpose, a combination of experimental characterization techniques, to study the pore solution composition and microstructure of SS-AAS pastes and thermodynamic calculations have been applied.

The initial precipitation of ill-defined N-A-S-H and C-N-A-S-H producta leads to a fast increase of the storage modulus after 40 min of reaction. These products are formed from the reaction of the Na^{+} ions and silicate ions of the activator with the Ca^{2+} and aluminate species dissolved from the slag. However, when a shear is applied, the structure breaks down and fluidity is recovered, that infers that the attractive forces between the particles are low at the early stages of hydration.

1. Introduction

For a concrete formulation to be acceptable, it is not sufficient to meet the mechanical strength, volume stability or durability requirements laid down in national and international standards. It must also be delivered on site with sufficient time for mixing, transport, casting and consolidation. This means that it must exhibit suitable workability and rheology [1,2].

Worldwide environmental concerns are driving the study and development of new construction materials with a lower carbon footprint. Alkali-activated cements and concretes are considered among such materials in which, compared to traditional cements and concretes, the portland clinker content of the binder is substantially lowered and replaced by industrial waste and by-products. Although many studies have been conducted on the mechanical strength and durability of alkali-activated binders [3–7], much fewer have explored their rheology [8]. One particularly intriguing phenomenon is the peculiar rheological behaviour of sodium silicate-alkali activated slag (SS-AAS) cementitious systems. Earlier studies showed that the workability and rheology of these materials are closely related to the alkalis concentration and silica modulus of the activating solution [9]. A faster loss of fluidity occurs as the SiO_2/Na_2O and the percentage of Na_2O increases. Furthermore, under a constant shear rate, a fast increase and consequent decrease of the shear stress was observed in SS-AAS pastes prepared with sodium silicate solutions containing 4% Na_2O and silica modulus between 1 and 1.5, while only a fast increase of the shear stress occured for silica modulus above 1.5 [9]. Palacios et al. [10] showed that lengthening mixing times improved the workability of SS-AAS systems, while enhancing mechanical strength and reducing drying shrinkage (a significant problem in these alkaline systems).

The rapid loss of workability and the especially short setting times observed in SS-AAS pastes, mortars and concretes have often been attributed to primary C-(A)-S-H formation, which would be the product of the immediate chemical reaction between the Ca^{2+} ions dissolving out of the slag into the highly alkaline medium and the silicate ions already present in the activator [11,12]. It has been hypothesized that the formation of this C-(A)-S-H would lead to the flocculation of the slag particles and to flow loss. However, empirical evidence of the existence of

the primary C-(A)-S-H has proved elusive to date, and this issue constitutes the key aim of this study.

For this purpose, the evolution of the composition of the pore solution and solids during the early reactivity of SS-AAS pastes was monitored and correlated with the time evolution of the rheological properties of the pastes during the first 5 h of reaction. Furthermore, the impact of the mixing time on the rheological properties of SS-AAS pastes has been explored. The new scientific understanding provided by this study will enable us in the future to develop new strategies to extend the workability of SS-AAS cements.

2. Experimental

2.1. Materials

A granulated vitreous blast furnace slag supplied by Ecocem (France) was used in this study. Its chemical composition was determined by X-ray fluorescence (XRF) using a Philips PW-1004 XRF spectrometer (see Table 1). Fig. 1 presents the particle size distribution of the slag dispersed in isopropanol measured by laser light scattering (Malvern MasterSizer S equipment) with a D_{v50} value of 10.42 μm.

A commercial sodium silicate solution (27.0 wt% SiO_2, 8 wt% Na_2O and 65 wt% H_2O; supplied by Merck) and NaOH (98% purity from Panreac) were used for the preparation of the activator solution. Sodium silicate, NaOH and ultrapure water (ρ = 18.2 MΩ·cm, TOC around 1–2 ppb) were mixed in the appropriate amounts to obtain an alkaline sodium silicate (SS) solution with 4% Na_2O by weight of slag, SiO_2/Na_2O = 1.5 and H_2O/Na_2O = 11.1. This solution composition was chosen because it has been reported in previous studies [9,12] to result in pastes with poor rheological properties.

2.2. Sample preparation and test performed

SS-AAS pastes were prepared by mixing at room temperature 80 g of blast furnace slag with 44 g of the alkaline sodium silicate activator (liquid/solid ratio = 0.55) for 30 s at 200 rpm with a mechanical stirrer using an anchor geometry (6 cm of diameter) in a plastic container with an internal diameter of 9 cm. The pastes were afterwards mixed during 3 min at 700 rpm. The test carried out on these pastes are described below.

2.2.1. Rheological behaviour

Three different rheological tests were carried out on SS-AAS pastes:

- Measurements at constant shear rate: Pastes were placed in a Haake Rheowin Pro RV1 rotational viscometer fitted with a grooved Z38/S cylindrical rotor blade. The evolution of the apparent viscosity of the SS-AAS pastes was tested for 70 min at a constant shear rate of 100 s^{-1} at 25 °C ± 0.1 °C.
- Small amplitude oscillatory shear (SAOS) measurements were carried out using a Malvern Kinexus Lab+, a stress-controlled rheometer equipped with serrated parallel plates [13] at room temperature (23 ± 0.1 °C). The diameter of the plates was 25 mm and the gap between plates was 1 mm. After mixing, the paste was poured on the lower plate of the rheometer before the upper plate was set into position and covered to limit evaporation. The sample was sheared at 100 s^{-1} for 30 s and after a 10 s resting time, the measurement sequence started. The limits of the linear viscoelastic range (LVR), where the rheological properties of the materials are not strain- or stress-dependent, were first determined by identifying the critical value of strain γ_c through a strain sweep test: a strain amplitude (from 0.0001% to 100%) at a constant frequency of 1 Hz was applied and the end of the linear elastic regime was defined as when the storage modulus G' falls to 90% of the plateau value [14]. The viscoelastic property G' (storage modulus) of the SS-AAS slag pastes was then investigated in a large time domain by applying for 70 min a constant shear strain (lower than γ_c) and a constant frequency of 1 Hz to the material, and by recording the subsequent stress. This test is used as an indication of the time-dependent structural changes within the material.
- Effect of the mixing time on the rheology of SS-AAS pastes: pastes were prepared by mixing 500 g of slag with 275 g of the alkaline sodium silicate solution as described in Section 2.2. ##Pastes were initially mixed at 200 rpm during 30 s and afterwards mixed during 3 or 5 min at 700 rpm. The evolution of the shear stress over time of the pastes was measured using a VISKOMAT NT (Schleibinger) equipped with a vane geometry and a constant shear rate of 100 s^{-1} was applied during the measurement. The use of this equipment enabled to test bigger batches of paste and confirm the anomalous rheological behaviour of SS-AAS pastes previously measured by using the Haake Rheowin Pro RV1 rotational viscometer.

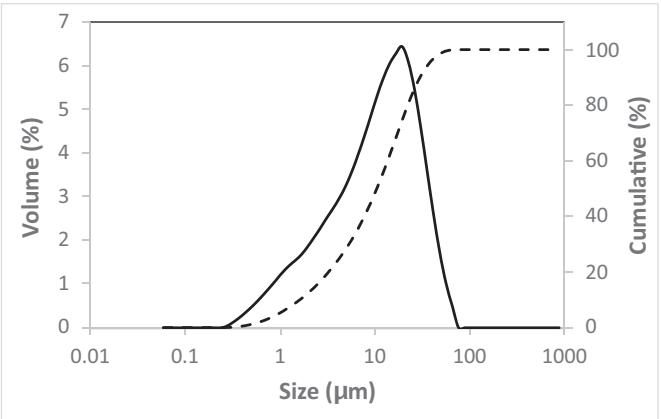

Fig. 1. Particle size distribution of the blast furnace slag.

2.2.2. Pore solution composition

SS-AAS pore solutions were extracted at different times by using the steel die method and filtered with a nylon 0.45 μm membrane filter. An aliquot of the samples was immediately acidified with HNO_3 2% wt. to prevent the precipitation of solids and analysed by Inductively Coupled Plasma – Optical Emission Spectrometry ICP-OES (VARIAN 725 ICP-OES). Pore solutions were diluted with HNO_3 2% wt. in a proportion of 1:50 to measure Al, Ca, Fe, Mg and K; and 1:2000 to measure Si and Na concentrations.

The pH of the pore solution was measured on the remaining solution at 25 °C ± 0.1 °C with a Crison pH meter (pH Basic 20). The electrode was calibrated with standard buffers (pH 4, 7 and 10). The measured pH values in the presence of 1 to 3 M Na are expected to underestimate the

Table 1
Chemical composition (wt%) of the blast furnace slag.

	CaO	SiO_2	Al_2O_3	MgO	Fe_2O_3	MnO	SO_3	Na_2O	K_2O	TiO_2	P_2O_5	LoI	IR
wt%	38.5	38.7	11.2	8.6	1.1	0.3	1.0	0.6	0.4	0.4	0.1	−1.0	0.0015

LoI: Loss on ignition measured at 1000 °C according to EN 196–2:2014. The negative value is due to the oxidation of sulphides to sulphates; IR: insoluble residue according to UNE 80230:2010.

real pH value by a factor of 0.3 to 0.5 pH units due to the alkali error caused by the presence of high Na-concentrations [15].

Moreover, static NMR ^{27}Al measurements were carried out on a Bruker Avance III 500 spectrometer at 11.7 T. Spectra were taken in a commercial static broadband Bruker probe. All spectra were recorded following a one pulse excitation with a recycle delay of 1 s and 80 number of transients. The pulse length was determined to be 3.75 μs by taking the maximum of the nutation curve of aluminium in a 0.1 M Al $(NO_3)_3$ aqueous solution. This solution also served as the external standard for calibrating the signal intensity and the chemical shift scale. The paste was introduced into a 5 mm diameter PTFE NMR tube immediately after mixing. At regular time intervals, the signal was recorded as the reaction progressed. Since the sample was not spinning, due to the strong quadrupolar coupling of ^{27}Al (a spin 5/2) in the slag, only the dissolved aluminium contributed to the signal. Solid reaction products of weak quadrupolar coupling might also contribute to a certain extent but this was neglected. This methodology has already been successfully applied to metakaolin geopolymer pastes [16]. The ^{27}Al resonance integrated intensity was calibrated with respect to an Al $(NO_3)_3$ aqueous solution of known concentration. As the liquid fraction of the sample is evolving over time as it is consumed during the hydration, the amount of Al in solution measured by NMR was not converted into an effective pore solution concentration.

2.2.3. Microstructure of pastes

Solvent replacement is the most widely applied method to stop the hydration of cementitious materials. However, organic solvents might interact with the silicates of the activator present in the pore solution of the pastes at early times; in SS-AAS pastes this was previously identified by Chen et al. [17]. In the present paper, a deeper study of the artefacts introduced by the organic solvents on SS-AAS microstructure has been done and an alternative method to stop of the reaction in fresh sodium silicate-activated materials has been applied.

The microstructure of quenched pastes was analysed at different reaction times over the first 5 h by the following techniques:

- Fourier-transform infrared spectroscopy (FTIR) spectra were obtained by using a Nicolet 6700 spectrometer (Thermo Scientific). KBr pellets were prepared by mixing 1 mg of sample and 200 mg of KBr. Frequencies were scanned in the range of 4000–400 cm^{-1}, with a resolution of 4 cm^{-1}.
- ^{29}Si and ^{27}Al magic angle solid nuclear magnetic resonance (MAS NMR) spectra were acquired on a BRUKER MSL 400 spectrometer. A 4-mm (outer diameter) ZrO_2 rotor was used at a spinning frequency of 10 kHz. The ^{29}Si and ^{27}Al spectra were obtained at resonance frequencies of 79.49 and 104.2 MHz, respectively. Chemical shift values were referenced to tetramethylsilane (TMS) and to a 1 M solution of $AlCl_3$ as external standards for ^{29}Si and ^{27}Al, respectively. In the ^{29}Si MAS NMR measurements the pulse length was 4.5 μs, the recycle delay 10 s and the number of scans 5600. For the ^{27}Al MAS NMR measurements the π/6 pulse length was 2 μs, the recycle delay 5 s and the number of scans 1200.
- SS-AAS pastes were observed by scanning electron microscopy (SEM) with a Hitachi S-4800 in secondary electrons mode, attached to an Bruker XFlash 5030 EDX microanalysis unit. Prior to imaging, the specimens were carbon coated.
- The BET surface area (SSA_{BET}) measurement was done using a BET multi-point nitrogen physisorption equipment (ASAP 2420). The samples were previously degassed in an external degassing station at 40 °C under N_2 flow for 16 h [18].
- Thermogravimetric analysis was performed with a TGA-DSC-DTA Q600 from TA Instruments. Around 40 mg of samples was heated in an alumina crucible from 30 to 1100 °C with a heating rate of 10 °C/min under N_2 atmosphere (100 ml/min).

2.3. Thermodynamic modelling

Gibbs Energy Minimization software (GEMS-PSI) [19] was used to determine the phase assemblage of the SS-AAS paste over the first 5 h of reaction. The GEMS-PSI [20] and the Cemdata18 [21] thermodynamic databases were used to calculate the solid phases precipitated; the C-N-A-S-H phase was modelled using the so-called "CNASH" model [21,22], which considers the uptake of alkali and aluminium in C-S-H phases. The data were completed with data for Na-containing zeolites [23]. It should be noted that the general thermodynamic database used in [20] describes the aqueous silica complexes at high silica concentration only poorly, due to the uncertainty associated with the data for polynuclear silica species. The formation of quartz, pyrite, goethite, and hematite in the hydrated cements was suppressed in the calculations for kinetic reasons. The composition of hydrated slag was modelled based on slag composition as determined by XRF data (Table 1) and the nominal composition of the sodium silicate solution used.

The measured concentrations of the pore solution were used to calculate the saturation index (*SI*) of different solids to assess which solids could potentially precipitate. The *SI* with respect to a solid is given by $\log(IAP/K_{S0})$, where *IAP* is the ion activity product calculated from activities derived from the measured concentrations in the solution and the solubility product, K_{S0}, of the respective solid [20]. A positive saturation index implies oversaturation indicating that the solid could form, while a negative value indicates undersaturation, the respective solid cannot form or will dissolve. As the use of saturation indices can be misleading when comparing phases, which dissociate into a different number of ions, "effective" saturation indices were calculated by dividing the saturation indices by the number of ions participating in the reactions [24]. The *SI* values for hydroxy-sodalite ($Na_8Al_6Si_6O_{24}(OH)_2{\cdot}2H_2O$), Na-chabazite ($Na_2Al_2Si_4O_{12}$ $6H_2O$), natrolite ($Na_2Al_2Si_3O_{10}$ $2H_2O$), and faujasite × ($Na_2Al_2Si_{2.5}O_9$ $6.2H_2O$), hydrotalcite ($Mg_4Al_2(OH)_{14}{\cdot}3H_2O$), CNASH (the *SI* were expressed with respect to $CaO(SiO_2)_{1.5}(Na_2O)_{0.3125}(H_2O)_{1.1875}$, the end-member of the C-N-A-S-H solid solution with the highest oversaturation), M-S-H, and strätlingite ($Ca_2Al_2SiO_2(OH)_{10}{\cdot}3H_2O$) were divided by 22, 8, 7, 6.5, 12, 4.75, 5.5 and 6 respectively to obtain effective *SI*. The activity coefficients of the aqueous species were calculated using the extended Debye-Hückel equation, which is applicable up to approx. 1 to 2 M ionic strength [25]:

$$log_{10}\gamma_i = \frac{-A_\gamma z_i^2\sqrt{I}}{1+\dot{a}B_\gamma\sqrt{I}} + b_\gamma I + log_{10}\frac{X_{jw}}{X_w}$$

γ_i represents the activity coefficient, z_i the charge of the species i, A_γ and B_γ are temperature- and pressure-dependent coefficients, I is the effective molal ionic strength, X_{jw} the molar quantity of water and X_w the total molar amount of the aqueous phase. Using NaOH as background electrolyte, the common ion size parameter $\dot{a}$ equals to 3.31 Å and b_γ, a short-range interaction parameter, to 0.098 [26].

3. Results

3.1. Rheological behaviour

Fig. 2 shows the evolution of the apparent viscosity of the SS-AAS pastes over the first 70 min of reaction. During the first 40 min, a steady decrease of the apparent viscosity was observed as the structure broke down with the applied shear. Afterwards, a sharp increase of the apparent viscosity occurred that reached a maximum at around 47 min, with a subsequent reduction of this rheological parameter. This rise of the viscosity occurred before the initial setting of the paste (occurring when a sufficient number of interparticle bridges are formed) at around 80 min (see Table S1 in supplementary material). However, it is worth highlighting that rheological and setting time measurements were carried out in different conditions, under a continuous shear in the former

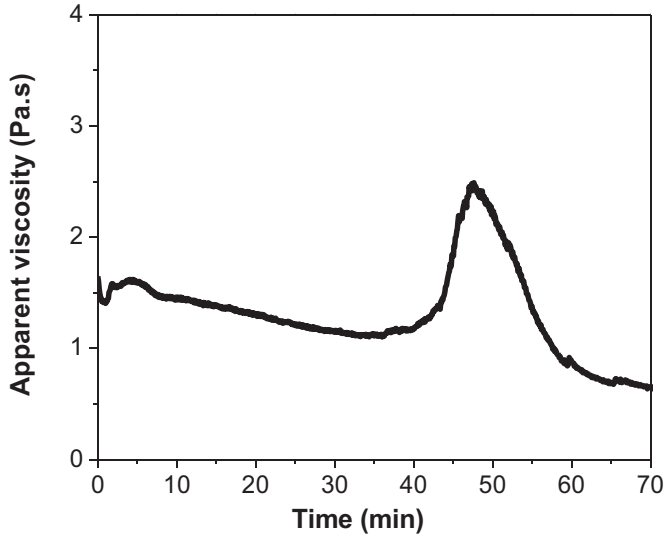

Fig. 2. Evolution of apparent viscosity over time in SS-AAS pastes. There is a transient increase of viscosity around 40 min. This was indicative of the temporary formation of a structure that eventually broke down under shear.

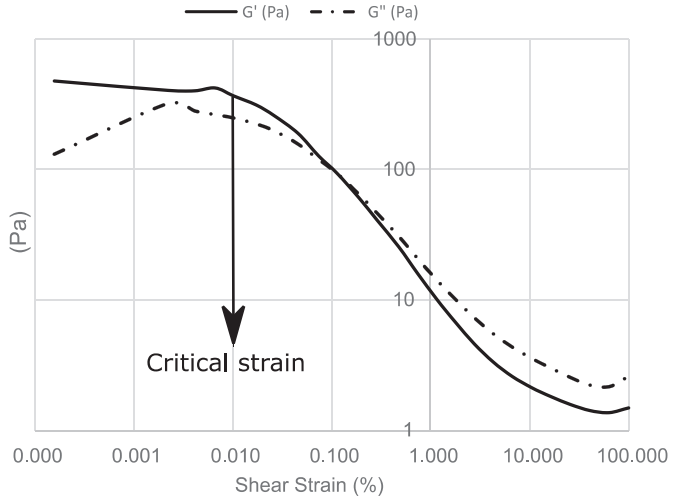

Fig. 3. Strain sweep of SS-AAS slag paste for the determination of the critical strain. Measurements were carried out immediately after the mixing stage. Log scales in both axis have been used.

and in static conditions in the latter. A similar evolution of the viscosity has been measured by using a Viskomat NT rheometer equipped with a vane geometry (see Fig. S1), confirming that no artefact was involved in this anomalous rheological behaviour.

The sharp increase of the viscosity could be related to (a) an increase of the viscosity of the interstitial fluid [11]; or (b) the interparticle bridges formed by the early reaction products growing onto the slag particles. Additional rheological tests performed on quartz sand (with a similar particle size distribution to the slag) mixed with the sodium silicate solution (the same than the one used in the preparation of SS-AAS pastes) have shown a constant apparent viscosity of the paste over the test (see Fig. S2 in Supplementary material). This meant that the rise of the viscosity of SS-AAS pastes was related to the initial chemical reactivity of the slag in contact with the alkaline solution. In fact, the calorimetry curve shown in Fig. S3 (in Supplementary material) showed after 30 min a first peak (with a maximum at 1 h) thus demonstrating the initial reactivity of the slag. This initial peak has been widely explained in the literature to correspond to the initial dissolution of the slag to form a primary C-S-H [11], something that we will further explore in this paper.

To gain further insights into the reaction and structuration of the pastes in its fresh state, SAOS measurements were carried out [27]. As shown in Fig. 3, where the storage modulus G' and the loss modulus G'' are plotted as a function of the strain, just after mixing, the SS-AAS paste had a critical strain γ_c of 0.01%. The critical strain establishes the limit of the linear viscoelastic regime (LVR) of the pastes: that is the strain at which the initial structure of the material has been sufficiently modified to produce the rupture of particle network of interactions [28]. The order of magnitude of the critical strain thus highlights the ability of the structural network to be deformed under stress and defines the nature of interactions. The small critical strain observed here, substantially lower than the one usually reported for Portland cement [29] or geopolymer systems [16], is associated with short range links between the particles [28]. Fig. 4 shows the evolution of the storage modulus G' over the reaction time at a constant shear strain of 0.005% (lower than γ_c). This parameter did not significantly change during the first 17 min of reaction, afterwards a slight increase was observed and a sharp rise of G' took place after 40 min of reaction. This indicated a fast structuration of the system after this time, at a time which matched the increase of the viscosity shown in Fig. 2. The measurement was stopped after 70 min, at which time, the modulus reached the limit of the rheometer at 300 kPa.

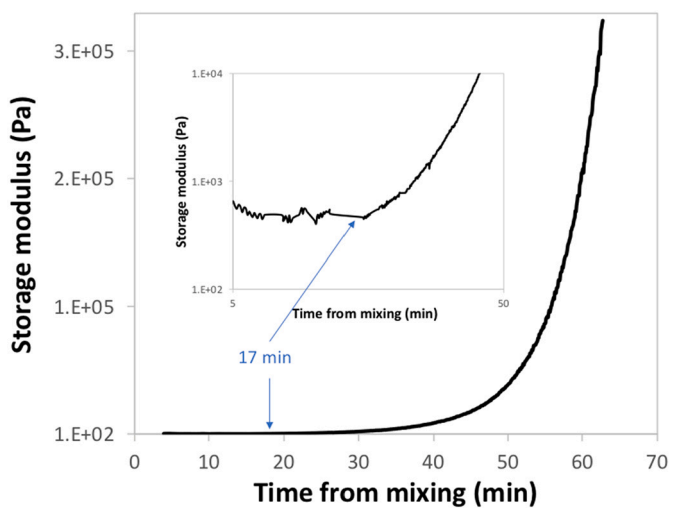

Fig. 4. Evolution of the storage modulus over time for the SS-AAS paste prepared using a sodium silicate solution with a $SiO_2/Na_2O = 1.5$ and 4%wt Na_2O by weight of slag.

3.2. *Pore solution composition*

3.2.1. *Analysis of the pore solution over time*

The evolution of the pH and composition of the pore solution of the SS-AAS paste over the first 5 h of reaction are shown in Table 2. The pH values remained almost constant over time, with a value between 13.1 and 13.3. An increase in the concentrations of Al, Ca and Mg was observed during the first 30 min because of the initial dissolution of the slag. Afterwards, a significant drop in the concentration of these elements, together with Na and Si, occurred. After 5 h of reaction the concentrations of Al, Ca and Mg were, respectively, 71%, 98% and 99% lower than those measured at 30 min. This was related to a change in the balance between the slag dissolution and the precipitation of the hydration products. It is worth highlighting, that the drop of these main elements in the pore solution occurred above 30 min, when the viscosity and the storage modulus increased (see Fig. 2 and Fig. 4).

In-situ monitoring of the aluminium species in the pore solution over time was performed by static liquid-state ^{27}Al NMR. This technique enables to detect primarily the aluminium in the pore solution while the signal coming from the solid phases is minimized. As shown in Fig. 5, at

Table 2
Measured composition of pore solutions from SS-AAS over the first 5 h of reaction.

Reaction time (minutes)	pH[a]	Al[b] (mmol/L)	Ca[b] (mmol/L)	Mg[b] (mmol/L)	Fe[b] (mmol/L)	Na[b] (mmol/L)	Si[b] (mmol/L)
15	13.1	17.20	47.77	16.37	0.46	2779	2173
30	13.2	27.75	69.61	23.00	0.49	2198	2187
60	13.2	22.97	24.85	9.16	0.11	1673	1567
90	13.2	18.25	6.58	3.01	0.01	1567	1356
120	13.3	16.34	3.17	2.44	0.01	1919	1076
180	13.3	12.74	3.83	1.13	0.03	1499	911
240	13.3	9.32	1.17	0.38	0.01	1169	563
300	13.3	7.90	0.70	0.21	0.00	1544	512

[a] The measured pH values in the presence of 1 to 3 M Na are expected to underestimate the real pH value by a factor of 0.3 to 0.5 pH units due to the alkali error [15].
[b] Measurement error ± 10%.

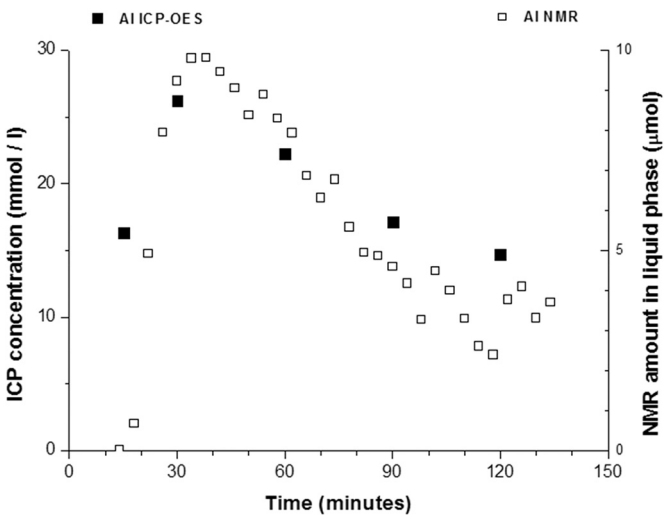

Fig. 5. Evolution of Al in the pore solution of SS-AAS pastes determined by ICP-OES (in mmol/l) and ^{27}Al MAS NMR (in µmol). ICP and NMR data cannot be directly compared since one measures a concentration and the other a quantity but the trends clearly matched.

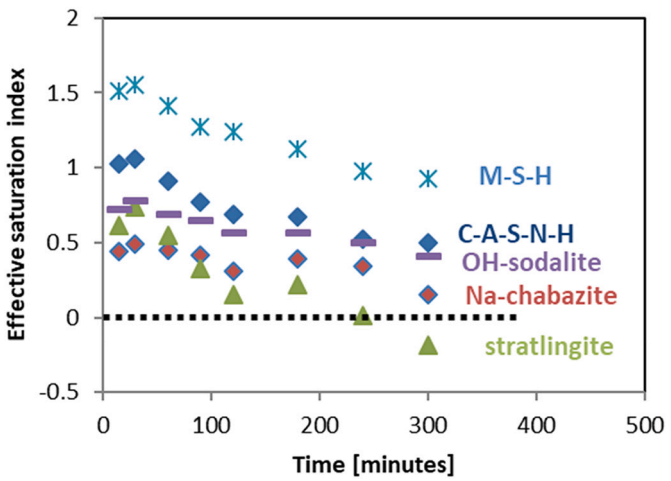

Fig. 6. Calculated effective saturation indices as a function of hydration time. A positive saturation index indicates oversaturation, a negative value undersaturation.

15 min of reaction, almost no tetrahedral aluminium species were detected in the interstitial fluid. Afterwards, an abrupt raise of the amount of aluminium signal occurred reaching a maximum at around 37 min. From that moment on, the amount of aluminium in solutions steadily decreased until 90 min of reaction, after which it remained constant within experimental error (±3 µmol). The evolution of Al in solution measured by ICP-OES and NMR matched and a drop of Al concentration is detected at the very moment when the elastic modulus of the paste increased.

3.2.2. *Effective saturation indexes over time in SS-AAS*

The determination of saturation indices from the concentrations determined in the pore solutions by ICP-OES offers the possibility of assessing independently which solid phases could form or are expected to dissolve. The effective saturation indices are plotted in Fig. 6. The positive SI values show that the solutions were at all-time oversaturated with respect to M-S-H, C-N-A-S-H and several Na-containing zeolites: hydroxy-sodalite ($Na_8Al_6Si_6O_{24}(OH)_2{\cdot}2H_2O$), natrolite ($Na_2Al_2Si_3O_{10}$ $2H_2O$), Na-chabazite ($Na_2Al_2Si_4O_{12}$ $6H_2O$) and faujasite X (Na_2Al_2-$Si_{2.5}O_9$ $6.2H_2O$), indicating that these solids could potentially form. The solutions were also oversaturated with respect to brucite, hydrotalcite and siliceous hydrogarnet ($Ca_3Fe_2(SiO_4)_{0.84}$ $(OH)_{8.64}$); data not shown. The positive effective saturation indices suggest that strätlingite could precipitate during the first hours, when the Al concentrations are relatively high, but any strätlingite would be destabilised at later ages when the solutions become undersaturated (negative SI).

The calculated saturation indices generally increased with time up to 30 min, but showed a decrease after 60 min indicating the nucleation of solids within this timeframe, consistent with the observed changes in viscosity and storage modulus.

3.3. *Arrest of the reaction of sodium silicate-activated slag pastes*

To correlate the rheological properties of SS-AAS pastes with the formation of hydration products over time, it is essential to effectively arrest the reaction of the pastes to be analysed without introducing artefacts. This is a relevant issue at early stages when high concentration of silicates is found in solution that might interact with organic solvents.

3.3.1. *Solubility of sodium silicate solution in organic solvents*

The solubility of the sodium silicate solution in organic solvents, commonly used to stop cement hydration such as acetone, ethanol and isopropanol was initially investigated. Organic solvent – sodium silicate mixes with a weight ratio of 1:10 and 1:1 were prepared; the former shown in Fig. 7 while the latter in Fig. S4 in the supplementary material. After contact of both compounds, the solution became turbid and a gel-type product formed at the bottom of the glass tubes. The amount of gel-type product depended on the type and amount of organic solvent, being the highest for ethanol-containing mixes and increasing with the solvent content. This observation agreed with previous studies [30] that considered the hydrolysis and condensation reactions of sodium silicate in alcohol solvents such as ethanol.

Fig. 8 shows the FTIR spectrum of the sodium silicate solution and of the precipitate formed after contact with the organic solvents. The spectrum of the sodium silicate solution shows a main band at 1004 cm^{-1} assigned to Si—O asymmetric stretching vibration of $[SiO(OH)_3]^-$

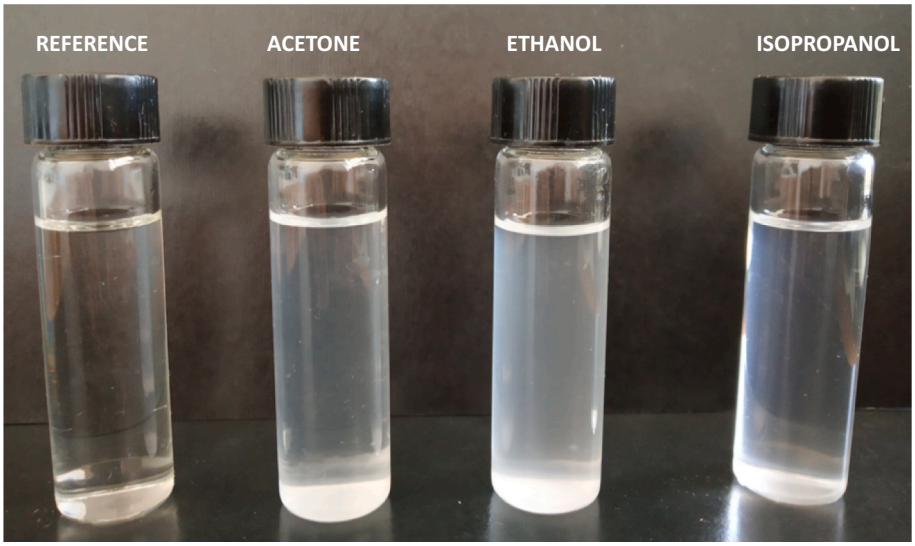

Fig. 7. Mixes of organic solvent:sodium silicate solution in a ratio of 1:10. The formation of a white gel-type product is observed. Reference tube contains exclusively the alkaline sodium silicate solution (SS).

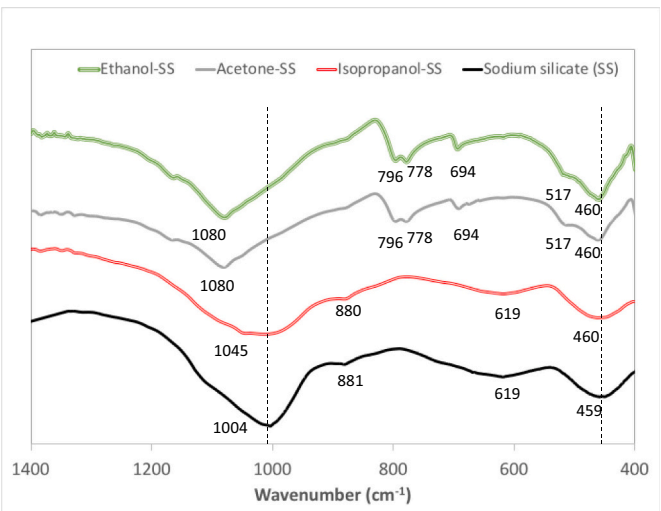

Fig. 8. FTIR spectra of the alkaline sodium silicate solution (SS) before and after treatment with ethanol, acetone and isopropanol in a ratio of organic solvent:SS of 1:1.

and $[SiO_2(OH)_2]^{2-}$ (Q^1 and Q^2, respectively) species and two bands at 459 and 619 cm^{-1} associated to the deformation of Si-O-Si of various Q^n species [31]. The FTIR spectra of the precipitate showed a shift of the band associated to the asymmetric stretch of Si—O from 1004 to 1040–1080 cm^{-1} with respect to the initial sodium silicate solution that confirmed the higher polymerization degree of the precipitated product with respect the starting sodium silicate solution.

The possible formation of this condensation product on the slag surface might introduce several artefacts during the characterization of fresh SS-AAS pastes (see Figs. S5 and S6 in the supplementary material). Therefore, an alternative method, described in the section below, has been used to stop the reactivity of SS-AAS pastes.

3.3.2. *Method to stop reaction of fresh SS-AAS pastes*

SS-AAS pastes were prepared as described in Section 2.2 and after 12 min of reaction, three different methods to stop the reaction were applied:

3.3.2.1. Solvent replacement with acetone and ethanol. The paste was initially treated during 45 s with acetone using a paste:solvent ratio of 3:10. Afterwards the solvent was vacuum filtered through a nylon filter with a size pore of 0.45 μm and the acetone treatment was repeated once. Finally, the solid was treated with 10 ml of ethanol during 15 s. After further filtration, the solid was vacuum filtered and dried in a desiccator under vacuum until constant weight.

3.3.2.2. Freeze-drying. SS-AAS paste was directly submerged into liquid nitrogen and after 1 h introduced in a freeze dryer device (TELSTAR CRYODOS) that keeps the temperature at −25 °C and pressure at 17 mPa. The sample was removed after 24 h.

3.3.2.3. Water and isopropanol treatment. SS-AAS paste was firstly mixed with ultrapure water, ρ = 18.2 MΩ·cm, TOC around 1–2 ppb, (1 g of paste and 20 g of ultrapure water). The solid was vacuum filtered, and the water treatment repeated. With this procedure, the non-reacted sodium silicate was removed and the reaction of the slag stopped. After vacuum filtration, the solid was washed with isopropanol (solid:isopropanol = 1:10), filtered and transferred to a desiccator under vacuum until constant weight. A similar procedure was previously proposed by Chen et al. [17]. We further discuss the benefits of using this alternative method in comparison with standard protocols used for Portland cement systems.

The obtained solids were analysed by SEM, TGA, FTIR and N_2 adsorption techniques. From the micrographs in Fig. 9a, the presence of a precipitate on the surface of the slag treated with acetone-ethanol can be observed. This may be attributed to the precipitation of the silicate species in alcohol and acetone [17] described in Section 3.3.1. Furthermore, a layer of an unknown product is detected on the slag surfaces when the freeze-drying method is applied (see Fig. 9b). The formation of this layer is not observed when slag is activated with NaOH and freeze dried as shown in Fig. S7 (supplementary material); which suggests that the sodium silicate solution was the main responsible for this artefact. With both treatments, the formation of products on the slag surface leads to a decrease of the SSA_{BET} with respect to the starting slag. In particular, SSA_{BET} decreased from the initial 1.27 m^2/g to 0.7–0.5 m^2/g (see Table 3). In addition, a weight loss of around 4% has been measured for the samples treated with acetone-ethanol and freeze-drying; which is rather high weight loss for samples that have only reacted over 12 min with typically small amount of reaction products.

In contrast, no precipitate was identified in samples treated with

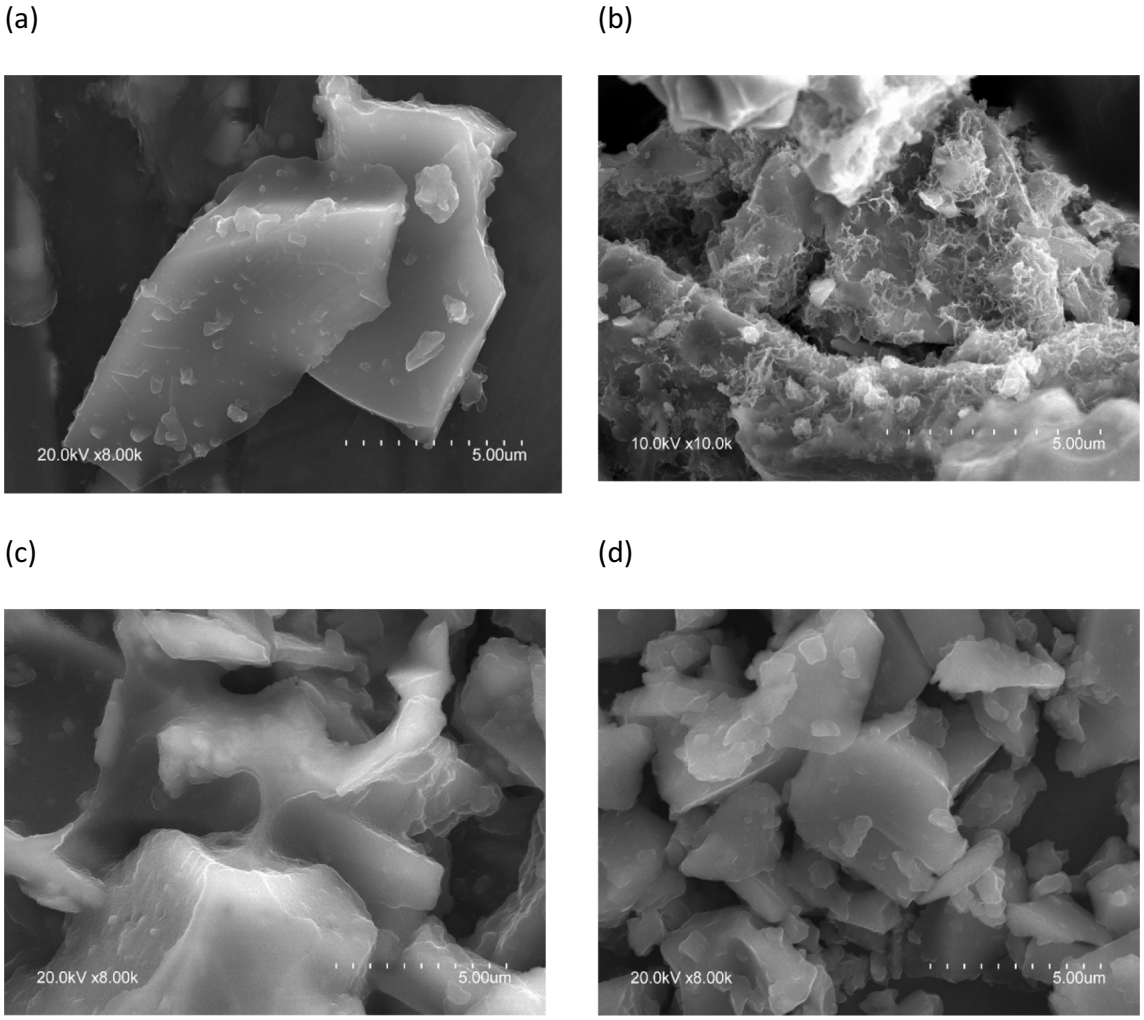

Fig. 9. (a) Starting blast furnace slag and slag particles after treatment of the SS-AAS pastes with: (b)Acetone-Ethanol; (c) Freeze-drying and (d) Water-isopropanol. SS-AAS pastes were tested after 12 min of reaction.

Table 3
SSA_{BET} of SS-AAS pastes after 12 min of reaction using different methods to stop their reaction. The starting slag has a SSA_{BET} of 1.27 m^2/g and a weight loss of 0.2%.

Method to arrest the reaction	Acetone–Ethanol	Freeze drying	Water-isopropanol
SSA_{BET} (m^2/g)	0.73	0.57	1.52
Weight loss (%) determined by TGA	3.8	4.3	0.3

water-isopropanol, leading to a similar SSA_{BET} as observed for the initial slag, and to a small weight loss in the TGA analysis that fits with the early studied hydration time (12 min).

Fig. 10 shows the FTIR spectra for the anhydrous slag and the pastes 20 min after exposure to different treatments. The very wide band observed in all cases between 730 cm^{-1} and 1200 cm^{-1} was associated with the υ_3 (Si—O) stretching vibrations in the SiO_4 tetrahedra [6]. The spectra exhibited a second wide band at 509 cm^{-1}, generated by the bending vibrations (υ_4 (O-Si-O)) [32]. The asymmetric stretching vibration bands attributed to the Al—O bonds in the AlO_4 groups present in the slag appeared at 700 cm^{-1} to 690 cm^{-1} [33].

A comparison between the spectra for the anhydrous slag and the SS-AAS pastes after different treatments revealed the band at 730 cm^{-1} to 1200 cm^{-1} to be significantly wider in two types of samples, those

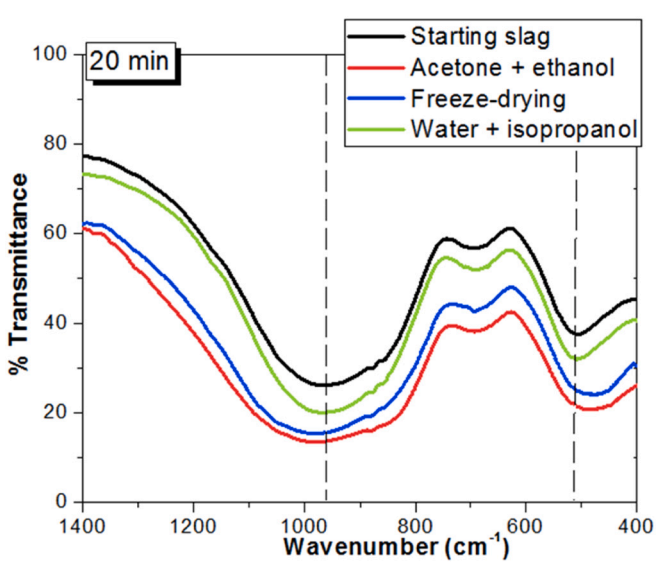

Fig. 10. FTIR spectra of the SS-AAS pastes treated with: (a) Acetone-Ethanol; (b) Freeze-drying and (c) Water-isopropanol. SS-AAS pastes were tested after 20 min of reaction.

treated with acetone and ethanol and those exposed to freeze-drying. That broader band would denote the presence of a lower order reaction product, such as a gel containing the organic solvents (see Fig. 8) or the layer of sodium silicate visible in in the freeze-dried samples (Fig. 9c). In contrast, the bands attributed to the Al—O bonds in the AlO_4 groups appeared to remain unaltered in the pastes, irrespective of the method used to stop the slag reaction.

The above results led to the conclusion that the initial washing of the SS-AAS pastes with water and subsequent treatment with isopropanol is the best method to arrest the reaction of SS-AAS pastes at early ages. Contrary to the organic solvent exchange and freeze-drying methods, no precipitates have been detected on the slag surface. Consequently, this alternative method was chosen to investigate the evolution of microstructure of early SS-AAS pastes in the next section.

3.4. Microstructural characterization of pastes over time

Table 4 shows the weight loss in the temperature range between 50 °C and 500 °C attributed to the bound water of the initial hydrates for the SS-AAS pastes over the first 5 h of hydration. The four samples showed a mass loss peak at around 650 °C attributed to the presence of $CaCO_3$ in the initial slag due to its weathering; the TGA curves are shown in Fig. S8 in the supplementary material.

At 12 min, the weight loss was very similar to the one of the starting slag, confirming the low advancement of the reaction at this age. In contrast, after 46 min and 5 h of reaction, a weight loss of around 2% and 4%, respectively, were measured that infers the formation of reaction products at the time when the storage modulus and viscosity of SS-AAS pastes dramatically rises.

Fig. 11 shows the FTIR spectra (in the 1700–400 cm^{-1} region) of the starting slag and the SS-AAS pastes up to 5 h of reaction. The spectra for the 9 min and 20 min pastes were very similar to the spectrum for the anhydrous slag, further confirming the low degree of reaction at such short activation times. After 46 min and 60 min, both the υ_3 (Si—O) (at around 968 cm^{-1}) and the υ_4 (O-Si-O) (at around 500 cm^{-1}) bands widened, denoting lower short-range structural order in the pastes studied. Five hours into the reaction, the υ_3 (Si—O) band at 980 cm^{-1} was narrower and shifted to higher wavenumbers than in the original slag, indicating the formation of more highly polymerized reaction products.

The ^{29}Si MAS NMR spectra for the anhydrous slag and its hydrated pastes are reproduced in Fig. 12, whilst the spectrum for the sodium silicate solution used to activate the slag is shown in Fig. S9. The decomposition results are given in Table 5. The anhydrous slag was the primary source of the signal at −75.5 ppm in all the samples. In addition, a broad shoulder was present after 46 min. It was centered around −85.5 ppm extending between about −80 ppm and − 105 ppm. This chemical shift range corresponds to the resonances of the Q^n (mAl) (n = 1,2,3,4 and m = 0, 1, 2 3) units associated with all the silica containing moieties outside the slag (in slag, mainly Q^0 environments are present [34]), namely the solution silicate oligomers (at around −92 ppm) and the alumino-silicate gel, at around −89 ppm (Q^3(1Al)) and – 99.5 ppm (Q^4(4Al)) [16]. The signals associated with C-A-S-H would also overlap with this region, so we cannot totally discard the presence of a small amount of C-A-S-H at this reaction time. After 5 h, the intensity of the signal at −85.5 ppm increased. Consequently, the evolution of the ^{29}Si MAS NMR spectra were associated with alumino-silicate gel [16] and C-A-S-H product, which would increase with reaction time.

Table 4
Weight loss (%) of the starting slag and SS-AAS pastes at different reaction times measured by TGA.

Range of temperature (°C)	Weight loss (%)			
	Starting slag	SS-AAS pastes		
		12 min	46 min	5 h
25–500	0.25	0.34	1.96	3.82
500–1000	0.50	0.38	0.58	0.57

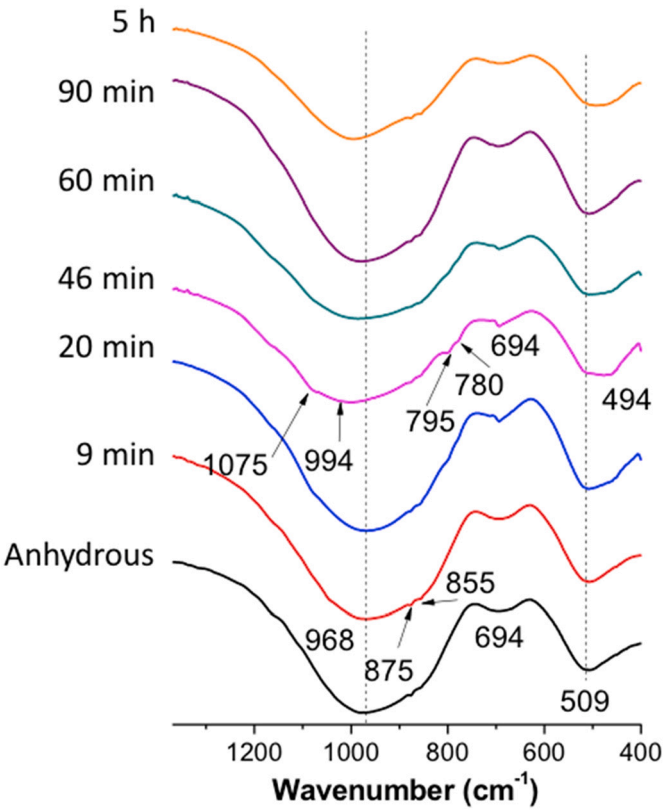

Fig. 11. FTIR spectra of the SS-AAS over time.

The 5 h ^{27}Al MAS NMR spectra obtained for the anhydrous slag and the SS-AAS pastes are reproduced in Fig. 13. The main peak narrowed as reaction proceeded. In glass, the breadth of the resonance of quadrupolar nuclei can be directly related to structural disorder via the Czjzek model [35]. Consequently, the observed narrowing could be due either to the passage of aluminium from a vitreous environment to a more organized C-A-S-H one, or to the preferential dissolution of the more disordered fractions of the slag. Actually, both phenomena are likely to occur simultaneously.

The microstructural surface of the slag particles was characterised by scanning electron microscopy (SEM) before and during the reaction with the sodium silicate solution (see Fig. 14). The SEM micrographs showed that the slag particles roughened as the reaction proceeded. After 46 min a very compact granular structure could be distinguished across the entire surface of the slag particles. This would confirm the formation of hydrates on the slag surface from around 40 min of slag reaction.

3.5. Thermodynamic modelling

Thermodynamic modelling was also used to calculate the kind and amount of hydrates that can be expected to form upon slag reaction as summarised in Fig. 15. The main hydrates predicted are C-N-A-S-H containing Na and Al, and a zeolitic precursor (here represented by hydroxy-sodalite), in agreement with different experimental and modelling results [36]. In addition, a minor amount of M-S-H, brucite and FeS (troilite) are predicted; the formation of a hydrotalcite like phase is predicted at above 20% slag reaction. The formation of C-A-S-H and hydrotalcite is observed commonly in alkali activated slags [37], as well as the precipitation of ill-defined N-A-S-H instead of a crystalline zeolite [3]. The formation of ill-defined and rather disordered tetrahedral-coordinated aluminosilicates is more likely to occur on

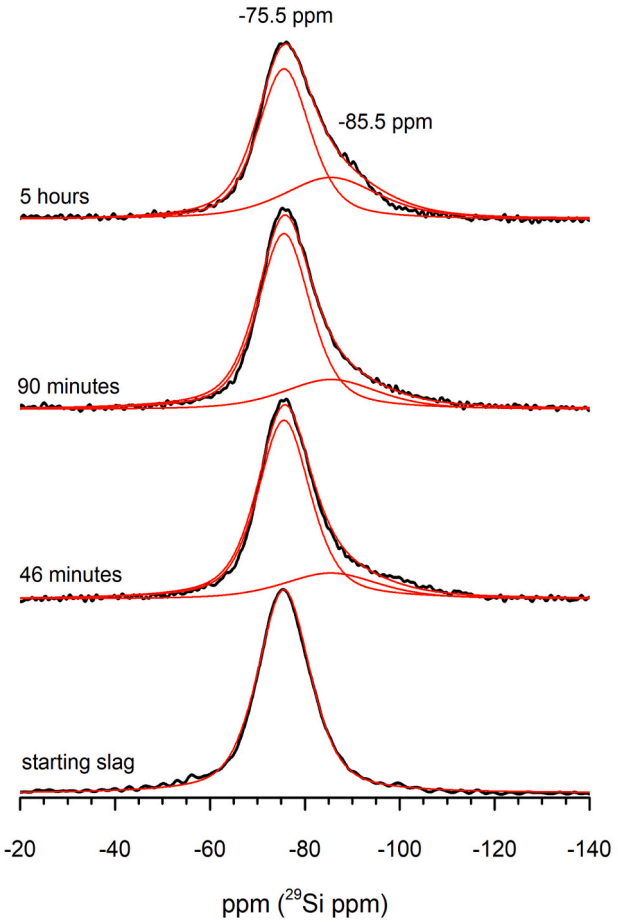

Fig. 12. ^{29}Si MAS NMR spectra of the starting slag and SS-AAS pastes over 5 h of reaction. Subtracting the contribution of the slag from the spectra reveals resonances in the range of −85 ppm corresponding to alumino-silicate gels and C-A-S-H; their intensity increased with time.

Table 5
Analysis of the ^{29}Si MAS NMR spectra of the starting slag and SS-AAS pastes over 5 h of reaction.

	Starting slag	46 min	90 min	5 h	Assignment
δ (ppm)	−75.5	−75.5	−75.5	−75.5	Q^0
Width (ppm)	13	13	13	13	
Integral (%)	100	79	77	66	
δ (ppm)		−85.5	−85.5	−85.5	Unresolved hydrates and silicate oligomers
Width		24	24	24	
Integral (%)		21	23	34	

shorter timeframes instead of crystalline zeolites as their formation is kinetically limited [38]. Thus, at early times, where we have a low degree of slag reaction of up to 20% the formation of ill ordered N-A-S-H gel and C-N-A-S-H, in agreement with the NMR results, can be expected to dominate the hydrates formed and thus the rheological properties.

4. Discussion

Several studies [9,39,40] have addressed the poor rheological properties of SS-AAS cementitious systems, that worsen with the increase of siliceous modulus and alkali concentration [9]. The formation

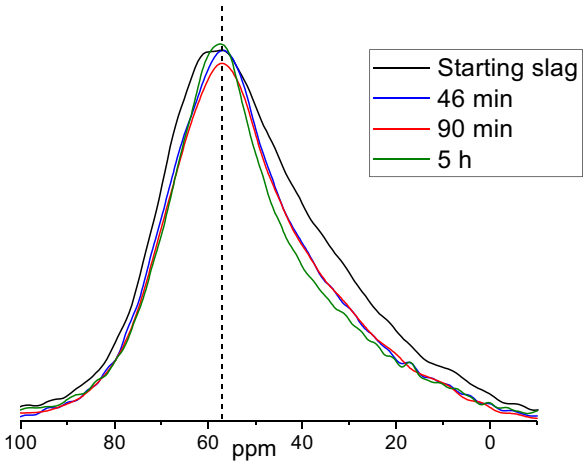

Fig. 13. ^{27}Al MAS NMR of the SS-AAS pastes at different reaction times. The resonances narrowed with time indicating the formation of products with higher ordering and aluminium site symmetry than the original slag.

of an early C-(A)-S-H has been pointed as the main responsible of the fast loss of fluidity of SS-AAS cements, however, no experimental evidences for that have been shown up to date. In this study, we correlate the rheology of SS-AAS systems with the evolution of the pore solution composition and hydration products formed over time. Furthermore, the impact of the mixing time on the rheological properties of these alkaline cements was investigated.

In a first step, an alternative protocol to stop the early reaction of SS-AAS had to be developed, as the sodium silicate in the pore solution precipitates in the presence of organic solvents normally used to stop the reactivity of Portland cements (see Figs. 7 and 8). Two consecutives washing of the SS-AAS pastes with ultrapure water (in a solid:water ratio 1:20) and a subsequent treatment with isopropanol and vacuum drying have been proved to be an optimum way to stop the early reactivity of SS-AAS without introducing artefacts. This method is mainly suitable for fresh samples (with high content of silicates in the pore solution). Otherwise, organic solvent exchange can be used in SS-AAS systems with longer reactions times and low silicate concentration in solution.

4.1. Correlation between the rheological properties and the evolution of the pore solution composition and reaction products

Small amplitude oscillatory shear measurements have enabled to monitor the structuration of SS-AAS pastes with a solution containing $SiO_2/Na_2O = 1.5$ and 4% Na_2O by weight of slag. Over the first 30–40 min of reaction, an increase of aluminate species, Ca and Mg, due to slag dissolution, was measured by ^{27}Al NMR and ICP-OES (Fig. 5 and Table 2). At this stage, FTIR and NMR analysis confirmed the absence of hydration products, explaining an almost constant value of the measured storage modulus (see Fig. 4). However, after 30–40 min of reaction, a drastic drop of the concentrations of Al, Si, Ca and Mg in the pore solution occurred, indicating a supersaturation of the solution and the precipitation of reaction products that led to a sharp increase of the storage modulus of SS-AAS. By ^{29}Si MAS NMR (Table 5), the proportion of silicon of unreacted slag is estimated to be only about 79%. Since the initial amount of silicon in slag in the reaction mixture was 86% (the rest coming from the activator), that means that the advancement of hydration of the silicate part of the slag at 45 min was 8%. This number, obtained by ^{29}Si NMR, does not consider aluminates but can be taken as rough estimate of the advancement of slag reaction. This amount of hydration products was small but enough to modify the structure of the paste.

The combination of FTIR and NMR measurements together with thermodynamic modelling has enabled us to identify the nature of these

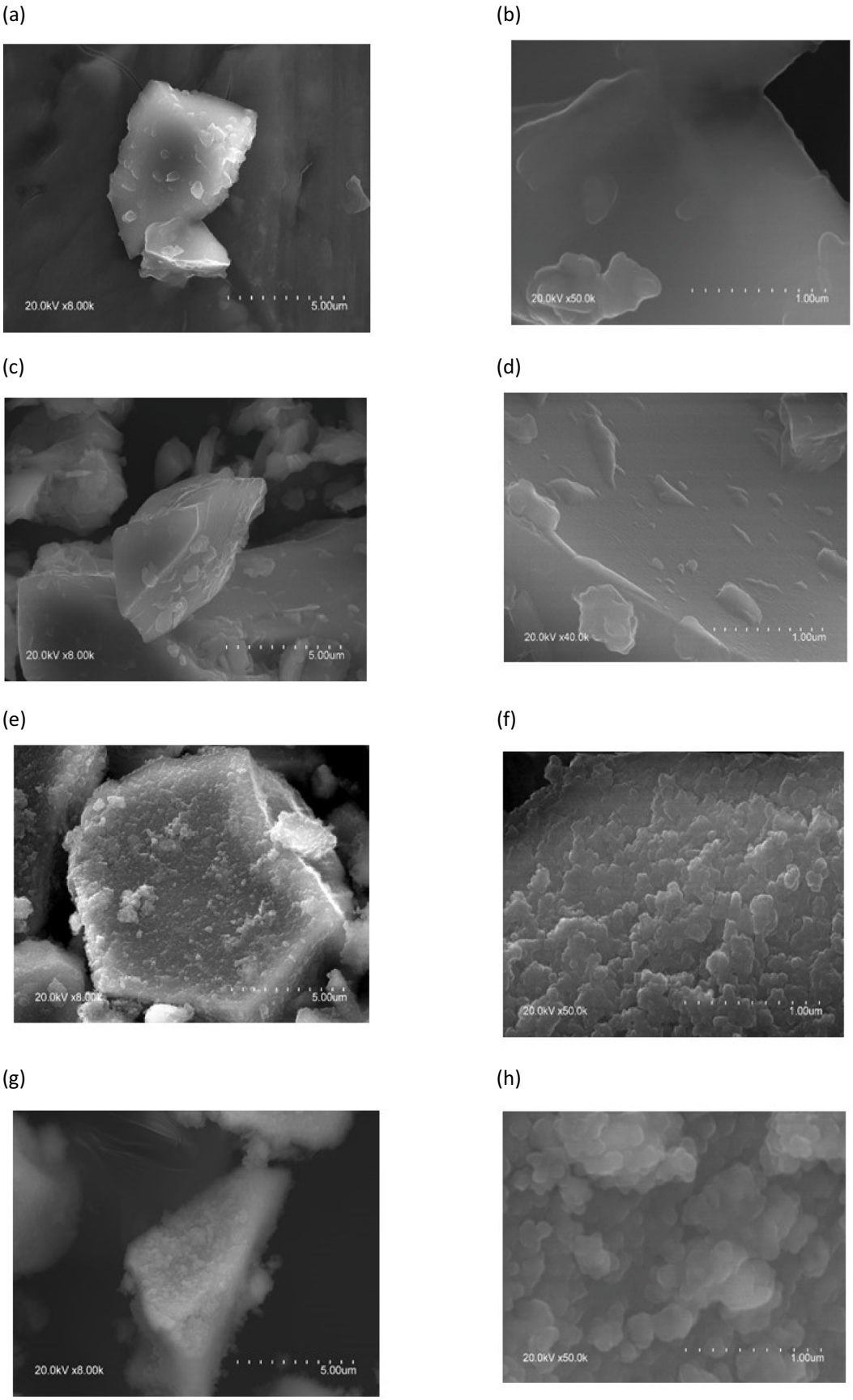

Fig. 14. SEM image of the starting slag and SS-AAS over 5 h of reaction; (a, b) starting slag; (c, d) at 12 min; (e, f) at 46 min and (g, h) at 5 h. After 46 min, the formation of reaction products is observed on the slag surface.

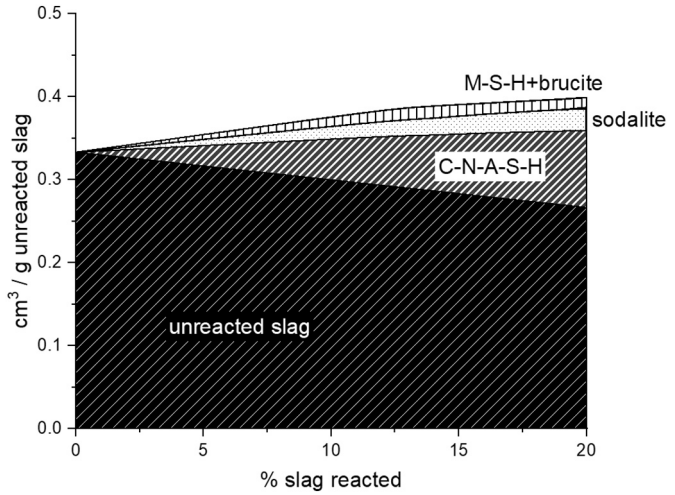

Fig. 15. Modelled volume of hydrates formed in the sodium silicate containing solution as a function of the degree slag reaction. The formation of a poorly ordered N-A-S-H precursor gel instead of the calculated OH-sodalite is expected.

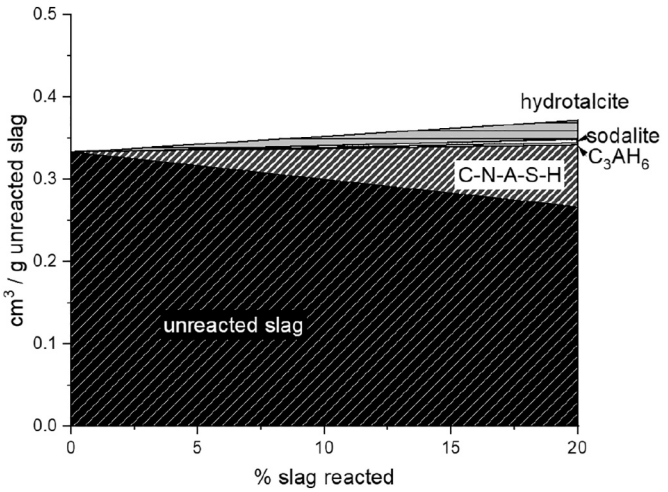

Fig. 16. Modelled volume of hydrates formed in the NaOH-AAS pastes (with 4%wt Na_2O by weight of slag) as a function of the degree slag reaction.

early hydration products. After 40 min of reaction, FTIR (Fig. 11) and ^{29}Si MAS NMR (Fig. 12) data confirmed the formation of a reaction product highly polymerized, in particular, a broad signal centred at around −85 ppm in the ^{29}Si MAS NMR could indicate the formation of an aluminosilicate gel and C-A-S-H. This agrees with the thermodynamic modelling results that predicts, at the early stages of the slag reaction, the co-existence of an ill-defined N-A-S-H and C-N-A-S-H. Both, the ill-defined N-A-S-H and C-N-A-S-H formed from the reaction of the Na^+ and silicate species originally in the solution with the Ca^{2+} ions and aluminate species dissolved from the slag. The removal of Mg and silicate ions can be also linked to the precipitation of M-S-H as predicted by thermodynamic calculations; however, this might be present in very low amounts, and it was not detected by FTIR or NMR. At 5 h of reaction, the amount of hydration products increased as shown in the FTIR spectra (Fig. 11) and ^{29}Si MAS NMR (Fig. 12). In particular, the FTIR spectra showed a narrowing of the υ_3 (Si—O) band at 980 cm^{-1} with the increase of the hydration time that indicates the formation of a more organized C-N-A-S-H, as also observed by ^{27}Al MAS NMR.

While in Portland cement systems the nucleation of C-S-H in the contact areas between particles leads to an increase in the shear modulus at very low degrees of hydration [29], in SS-AAS systems, the formation of an ill-defined N-A-S-H and C-A-S-H of a few nanometers is the main responsible of the rapid flow loss. The formation of an aluminosilicate gel has been also concluded to be the responsible for the increase of the elastic modulus in sodium silicate-activated metakaolin systems [16].

In contrast, in NaOH-AAS, no silicate species are initially in solution and the concentration of silicate and aluminium species as well as Ca ions slowly increases as slag dissolves. Thermodynamic calculations (shown in Fig. 16) predicted that no N-A-S-H is expected to form in such NaOH-AAS systems while experimental data indicated that the precipitation of C-A-S-H can take several hours [41], which together would explain why the NaOH-AAS systems remain fluid for longer time and have a longer setting times than SS-AAS systems.

The next question to address is, why does the viscosity decrease when a constant shear is applied to SS-AAS cements as observed in Fig. 2? According to the results, the slag starts to dissolve from the first moment of contact with the alkaline solution, releasing Ca, Al, Si and Mg into the pore solution. Once supersaturation is reached, a N-A-S-H precursor gel and C-(N)-A-S-H are formed leading to the flocculation of the particles. However, the attractive forces are relatively small, probably because of the low amount of hydrates formed, and a shear is able to break down the particles interaction. A sketch of the proposed mechanism is shown in Fig. 17. The use of sodium silicate solutions with a higher SiO_2/Na_2O and/or higher percentage of Na_2O would lead to the faster and higher amount of the reaction products, inducing higher attraction forces between particles that cannot overcome even by applying a constant shear as previously shown by Puertas et al. [9].

4.2. Impact of the mixing time on the rheological properties of SS-AAS pastes

An increase of the mixing time has been previously concluded to delay the setting times of SS-AAS [10]. For this reason, we have studied the effect of increasing the mixing time from 3.5 min to 5.5 min on the evolution of the shear stress of SS-AAS pastes. As shown in Fig. 18, an extension of 2 min of the mixing time delays around 30 min the time of appearance of the sharp increase of the shear stress (and consequently apparent viscosity). Again, the structure breaks down afterwards under shearing. The area under both curves is relatively similar independently of the applied mixing time (734 and 864 Pa·s, for pastes mixed during 3.5 and 5.5 min, respectively). However, a lower intensity of the peak is observed for pastes mixed for longer time. This might involve that the number of flocs formed over time is the same but they are formed at lower speed when pastes are mixed for a longer time.

The extension of the fluidity of SS-AAS systems is essential to easily place them in practice. Current superplasticizers have been proved to lose their dispersing properties when sodium silicate is used as activating solution in alkali-activated slag systems. Their lack of solubility in these alkaline solutions and the highly competitive adsorption between the superplasticizers and the silicates of the activating solution [42] are the main responsible of their ineffectiveness. As shown in this study, a longer mixing leads to an extension of the period where the system remains fluid, however, extra mixing is not enough and an alternative strategy must be found. From the results obtained in this study, we now understand that it is essential to identify effective retarding admixtures that delay the slag reactivity and the early formation of the N-A-S-H precursor gel and C-N-A-S-H. The addition of maleic acid [43] or nano-ZnO [44] has been probed in the literature to delay the reaction of sodium silicate-activated slag cements. While the former does not affect to the nature of the hydration products, the latter slows down the reactivity of the slag by forming calcium zincate at the early stage of the hydration and depleting the calcium in solution to form C-N-A-S-H. We need now to further expand these studies and understand the impact of effective retarders on the fluidity of SS-AAS cements.

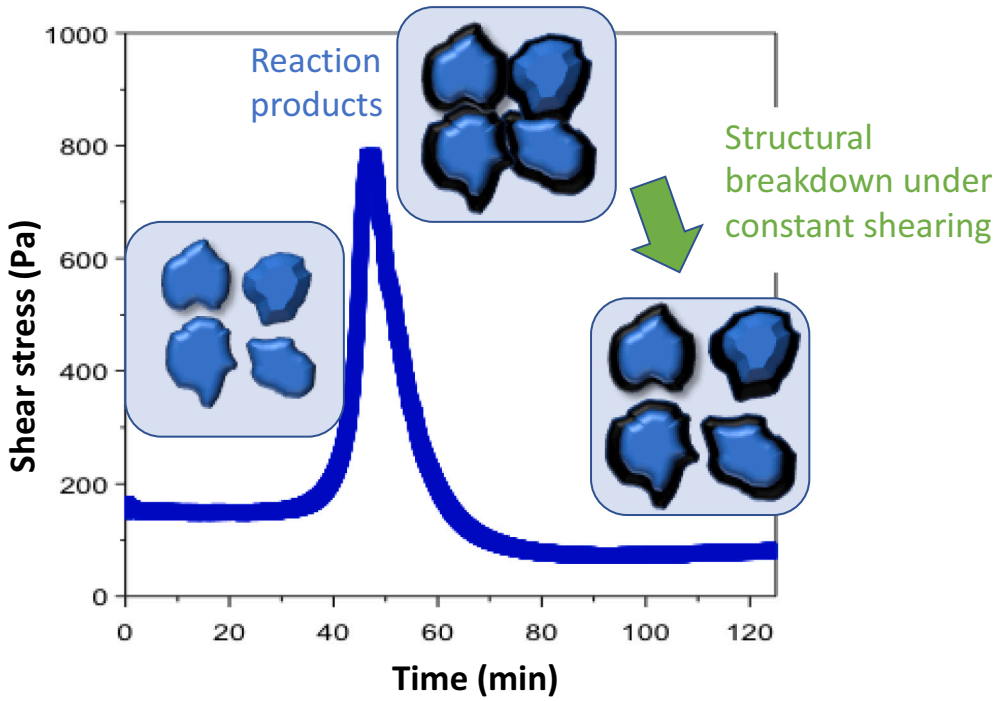

Fig. 17. Sketch of the mechanism behind the decrease of the shear stress of SS-AAS under constant shear. Full coverage of the slag particle with the reaction products is not required to induce their flocculation.

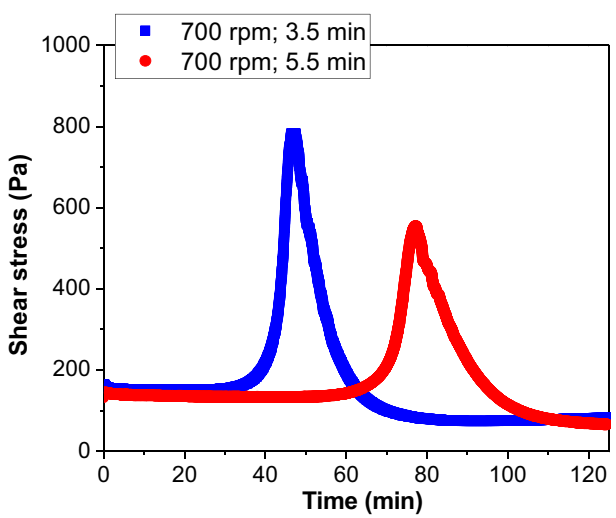

Fig. 18. Evolution of the shear stress over time in SS-AAS pastes prepared with mixing times of 3.5 and 5.5 min. A delay of 30 min in the time of appearance of the increase of the shear stress is observed as the mixing time increases.

5. Conclusions

In this paper, a combination of experimental characterization techniques, to study the pore solution composition and microstructure of SS-AAS pastes, and thermodynamic calculations have been applied to understand their anomalous rheological properties. The initial precipitation of an ill-defined N-A-S-H (precursor of N-A-S-H gel) and C-N-A-S-H cause the fast increase of the storage modulus, and loss of fluidity, after 40 min of reaction. Both reaction products are formed from the reaction of the Na^{+} ions and silicate ions in the initial activating solution with the Ca^{2+} and aluminate species dissolved from the slag.

If a shear is applied, the viscosity of SS-AAS pastes dramatically decreases after reaching a maximum value. This allows to infer that the attractive forces between the particles with the early hydrates are low, probably due to the small amount of reaction products formed at the early stages, and deflocculation takes place.

An increase of the mixing time delays the time at which the dramatic increase of the shear stress occurs and the flocculation rate of SS-AAS pastes.

An alternative method has been used to arrest the reaction of sodium silicate-activated slag (SS-AAS) pastes that involves an initial treatment of the SS-AAS pastes with water to remove the sodium silicate in solution and decrease the pH, and a subsequent treatment with isopropanol. This has been proved to avoid artefacts for the microstructural analysis of the SS-AAS pastes.

CRedit authorship contribution statement

Marta Palacios: Conceptualization, Methodology, Writing-original draft, Supervision, Funding adquisition; **Sara Gismera**: Investigation, Methodology; **M.M. Alonso**: Methodology, Supervision, Revision of the manuscript; **Jean-Baptiste d'Espinose de Lacaillerie**; Methodology, Writing-original draft, **Barbara Lothenbach**: Methodology, Writing-original draft; **Aurelie Favier**: Investigation, Revision of the manuscript; **Coralie Brumaud**: Investigation, Revision of the manuscript, **Francisca Puertas**: Conceptualization; Supervision; Writing-original draft, Project administration; Funding acquisition.

Declaration of competing interest

The authors declare that they have no known competing financial interests or personal relationships that could have appeared to influence the work reported in this paper.

Acknowledgement

The authors thank Prof. Habert (ETHZ) for constructive discussion. Dr. Francesco Caruso (SIK-ISEA) is thanked for helping to develop a protocol for the ICP-OES measurements. Dr. M. Palacios acknowledges

Consejería de Educación e Investigación (Comunidad de Madrid) for funding the 2016-T1/AMB-1434 project in the frame of "Ayudas de Atracción de Talento Investigador" and MCIU/AEI/FEDER, UE for funding the RTI2018-099326-A-I00 project. Prof. F. Puertas thanks the Spanish Ministry of Science and Innovation for funding BIA2013-47876-C2-1-P and BIA2016-77252-P projects.

Appendix A. Supplementary data

Supplementary data to this article can be found online at https://doi.org/10.1016/j.cemconres.2020.106302.

References

[1] G.H. Tattersall, P.F.G. Banfill, The Rheology of Fresh Concrete, Pitman, Advanced Publishing Program, 1983.
[2] K. Kovler, N. Roussel, Properties of fresh and hardened concrete, Cem. Concr. Res. 41 (2011) 775–792, https://doi.org/10.1016/j.cemconres.2011.03.009.
[3] J.L. Provis, S.A. Bernal, Geopolymers and related alkali-activated materials, Annu. Rev. Mater. Res. 44 (2014) 299–327, https://doi.org/10.1146/annurev-matsci-070813-113515.
[4] C. Shi, B. Qu, J.L. Provis, Recent progress in low-carbon binders, Cem. Concr. Res. 122 (2019) 227–250, https://doi.org/10.1016/j.cemconres.2019.05.009.
[5] A. Palomo, P. Krivenko, I. Garcia-Lodeiro, E. Kavalerova, O. Maltseva, A. Fernández-Jiménez, A review on alkaline activation: new analytical perspectives, Mater. Construcc. 64 (2014) 022.
[6] F. Puertas, S. Martinez-Ramirez, S. Alonso, T. Vázquez, Alkali-activated fly ash/slag cements: Strength behaviour and hydration products, Cement and Concrete Research 30 (2000) 1625–1632, https://doi.org/10.1016/S0008-8846(00)00298-2.
[7] R. Robayo-Salazar, R.M. de Gutiérrez, F. Puertas, Alkali-activated binary concrete based on a natural pozzolan: physical, mechanical and microstructural characterization, Mater. Construcc. 69 (2019) 191, https://doi.org/10.3989/mc.2019.06618.
[8] F. Pacheco-Torgal, J. Labrincha, C. Leonelli, A. Palomo, P. Chindaprasit, Handbook of Alkali-Activated Cements, Elsevier, Mortars and Concretes, 2014.
[9] F. Puertas, C. Varga, M.M. Alonso, Rheology of alkali-activated slag pastes. Effect of the nature and concentration of the activating solution, Cement and Concrete Composites 53 (2014) 279–288, https://doi.org/10.1016/j.cemconcomp.2014.07.012.
[10] M. Palacios, F. Puertas, Effectiveness of Mixing Time on Hardened Properties of Waterglass-Activated Slag Pastes and Mortars, MJ. vol. 108, 2011, pp. 73–78, https://doi.org/10.14359/51664218.
[11] Z. Huanhai, W. Xuequan, X. Zhongzi, T. Mingshu, Kinetic study on hydration of alkali-activated slag, Cem. Concr. Res. 23 (1993) 1253–1258, https://doi.org/10.1016/0008-8846(93)90062-E.
[12] M. Palacios, P.F.G. Banfill, F. Puertas, Rheology and setting of alkali-activated slag pastes and mortars: effect of organic admixture, MJ. 105 (2008) 140–148.
[13] P. Coussot, Rheometry of Pastes, Suspensions, and Granular Materials: Applications in Industry and Environment, Wiley, 2005.
[14] L. Nachbaur, J.C. Mutin, A. Nonat, L. Choplin, Dynamic mode rheology of cement and tricalcium silicate pastes from mixing to setting, Cem. Concr. Res. 31 (2001) 183–192, https://doi.org/10.1016/S0008-8846(00)00464-6.
[15] B. Traynor, H. Uvegi, E. Olivetti, B. Lothenbach, R.J. Myers, Methodology for pH Measurement in High Alkali Cementitious Systems, Cement and Concrete Research, Submitted, 2020.
[16] A. Favier, G. Habert, N. Roussel, J.-B. d'Espinose de Lacaillerie, A multinuclear static NMR study of geopolymerisation, Cem. Concr. Res. 75 (2015) 104–109, https://doi.org/10.1016/j.cemconres.2015.03.003.
[17] X. Chen, A. Meawad, L.J. Struble, Method to stop geopolymer reaction, J. Am. Ceram. Soc. 97 (2014) 3270–3275, https://doi.org/10.1111/jace.13071.
[18] S. Mantellato, M. Palacios, R.J. Flatt, Reliable specific surface area measurements on anhydrous cements, Cem. Concr. Res. 67 (2015) 286–291, https://doi.org/10.1016/j.cemconres.2014.10.009.
[19] D.A. Kulik, T. Wagner, S.V. Dmytrieva, G. Kosakowski, F.F. Hingerl, K. V. Chudnenko, U.R. Berner, GEM-Selektor geochemical modeling package: revised algorithm and GEMS3K numerical kernel for coupled simulation codes, Comput. Geosci. 17 (2013) 1–24, https://doi.org/10.1007/s10596-012-9310-6.
[20] T. Thoenen, W. Hummel, U. Berner, E. Curti, Thermodynamic Database 12/07, PSI report 14–04, Villigen PSI, Switzerland, 2014.
[21] B. Lothenbach, D.A. Kulik, T. Matschei, M. Balonis, L. Baquerizo, B. Dilnesa, G. D. Miron, R.J. Myers, Cemdata18: a chemical thermodynamic database for hydrated Portland cements and alkali-activated materials, Cem. Concr. Res. 115 (2019) 472–506, https://doi.org/10.1016/j.cemconres.2018.04.018.
[22] R.J. Myers, S.A. Bernal, J.L. Provis, A thermodynamic model for C-(N-)A-S-H gel: CNASH_ss. Derivation and validation, Cement and Concrete Research. 66 (2014) 27–47, https://doi.org/10.1016/j.cemconres.2014.07.005.
[23] B. Ma, B. Lothenbach, Synthesis, characterization, and thermodynamic study of selected Na-based zeolites, Cem. Concr. Res. 135 (2020) 106111, https://doi.org/10.1016/j.cemconres.2020.106111.
[24] B. Lothenbach, G. Le Saout, E. Gallucci, K. Scrivener, Influence of limestone on the hydration of Portland cements, Cem. Concr. Res. 38 (2008) 848–860, https://doi.org/10.1016/j.cemconres.2008.01.002.
[25] B.J. Merkel, B. Planer-Friedrich, Groundwater Geochemistry: A Practical Guide to Modeling of Natural and Contaminated Aquatic Systems, 2nd ed., Springer-Verlag, Berlin Heidelberg, 2008 https://doi.org/10.1007/978-3-540-74668-3.
[26] H.C. Helgeson, D.H. Kirkham, G.C. Flowers, Theoretical prediction of the thermodynamic behavior of aqueous electrolytes by high pressures and temperatures; IV, calculation of activity coefficients, osmotic coefficients, and apparent molal and standard and relative partial molal properties to 600 degrees C and 5kb, Am. J. Sci. 281 (1981) 1249–1516, https://doi.org/10.2475/ajs.281.10.1249.
[27] N. Roussel, H. Bessaies-Bey, S. Kawashima, D. Marchon, K. Vasilic, R. Wolfs, Recent advances on yield stress and elasticity of fresh cement-based materials, Cem. Concr. Res. 124 (2019) 105798, https://doi.org/10.1016/j.cemconres.2019.105798.
[28] N. Roussel, A. Lemaître, R.J. Flatt, P. Coussot, Steady state flow of cement suspensions: a micromechanical state of the art, Cem. Concr. Res. 40 (2010) 77–84, https://doi.org/10.1016/j.cemconres.2009.08.026.
[29] N. Roussel, G. Ovarlez, S. Garrault, C. Brumaud, The origins of thixotropy of fresh cement pastes, Cem. Concr. Res. 42 (2012) 148–157, https://doi.org/10.1016/j.cemconres.2011.09.004.
[30] C.Y. Jung, J.S. Kim, T.S. Chang, S.T. Kim, H.J. Lim, S.M. Koo, One-step synthesis of structurally controlled silicate particles from sodium silicates using a simple precipitation process, Langmuir. 26 (2010) 5456–5461, https://doi.org/10.1021/la904572y.
[31] J. Osswald, K.T. Fehr, FTIR spectroscopic study on liquid silica solutions and nanoscale particle size determination, J. Mater. Sci. 41 (2006) 1335–1339, https://doi.org/10.1007/s10853-006-7327-8.
[32] W. Mozgawa, J. Deja, Spectroscopic studies of alkaline activated slag geopolymers, J. Mol. Struct. 924–926 (2009) 434–441, https://doi.org/10.1016/j.molstruc.2008.12.026.
[33] G. Socrates, Infrared and Raman Characteristics Group Frequencies, 3rd Edition, John Wiley & Son Ltd., 2001.
[34] F. Puertas, M. Palacios, H. Manzano, J.S. Dolado, A. Rico, J. Rodríguez, A model for the C-A-S-H gel formed in alkali-activated slag cements, J. Eur. Ceram. Soc. 31 (2011) 2043–2056, https://doi.org/10.1016/j.jeurceramsoc.2011.04.036.
[35] J.-B. d'Espinose de Lacaillerie, C. Fretigny, D. Massiot, MAS NMR spectra of quadrupolar nuclei in disordered solids: the Czjzek model, J. Magn. Reson. 192 (2008) 244–251, https://doi.org/10.1016/j.jmr.2008.03.001.
[36] M.B. Haha, B. Lothenbach, G. Le Saout, F. Winnefeld, Influence of slag chemistry on the hydration of alkali-activated blast-furnace slag — part I: effect of MgO, Cem. Concr. Res. 41 (2011) 955–963, https://doi.org/10.1016/j.cemconres.2011.05.002.
[37] M. Ben Haha, G. Le Saout, F. Winnefeld, B. Lothenbach, Influence of activator type on hydration kinetics, hydrate assemblage and microstructural development of alkali activated blast-furnace slags, Cem. Concr. Res. 41 (2011) 301–310, https://doi.org/10.1016/j.cemconres.2010.11.016.
[38] B. Lothenbach, E. Bernard, U. Mäder, Zeolite formation in the presence of cement hydrates and albite, physics and chemistry of the earth, Parts A/B/C. 99 (2017) 77–94, https://doi.org/10.1016/j.pce.2017.02.006.
[39] F. Puertas, B. González-Fonteboa, I. González-Taboada, M.M. Alonso, M. Torres-Carrasco, G. Rojo, F. Martínez-Abella, Alkali-activated slag concrete: fresh and hardened behaviour, Cem. Concr. Compos. 85 (2018) 22–31, https://doi.org/10.1016/j.cemconcomp.2017.10.003.
[40] A. Kashani, J.L. Provis, G.G. Qiao, J.S.J. van Deventer, The interrelationship between surface chemistry and rheology in alkali activated slag paste, Constr. Build. Mater. 65 (2014) 583–591, https://doi.org/10.1016/j.conbuildmat.2014.04.127.
[41] K. Gong, Y. Cheng, L.L. Daemen, C.E. White, In situ quasi-elastic neutron scattering study on the water dynamics and reaction mechanisms in alkali-activated slags, Phys. Chem. Chem. Phys. 21 (2019) 10277–10292, https://doi.org/10.1039/C9CP00889F.
[42] D. Marchon, U. Sulser, A. Eberhardt, R.J. Flatt, Molecular design of comb-shaped polycarboxylate dispersants for environmentally friendly concrete, Soft Matter 9 (2013) 10719–10728, https://doi.org/10.1039/C3SM51030A.
[43] A.R. Brough, M. Holloway, J. Sykes, A. Atkinson, Sodium silicate-based alkali-activated slag mortars: Part II. The retarding effect of additions of sodium chloride or malic acid, Cement and Concrete Research. 30 (2000) 1375–1379, https://doi.org/10.1016/S0008-8846(00)00356-2.
[44] N. Garg, C.E. White, Mechanism of zinc oxide retardation in alkali-activated materials: an in situ X-ray pair distribution function investigation, J. Mater. Chem. A 5 (2017) 11794–11804, https://doi.org/10.1039/C7TA00412E.